Supporting Information

Enhanced Catalysis of Electrochemical Overall Water Splitting in Alkaline Media by Fe Doping in Ni_3S_2 Nanosheet Arrays

Geng Zhang,[a] Yu-Shuo Feng,[a] Wang-Ting Lu,[b,c] Dan He,[c] Cao-Yu Wang,[a] Yong-Ke Li,[a] Xun-Ying Wang[d] and Fei-Fei Cao*[a]

[a] Department of Chemistry, College of Science, Huazhong Agricultural University, 430070, Wuhan, P. R. China.

[b] Institute for Interdisciplinary Research, Jianghan University, 430056, Wuhan, P. R. China.

[c] Key Laboratory of Optoelectronic Chemical Materials and Devices, Ministry of Education, School of Chemical and Environmental Engineering, Jianghan University, Wuhan 430056, China.

[d] Collaborative Innovation Center for Advanced Organic Chemical Materials, Hubei Key Laboratory of Ferro & Piezoelectric Materials and Devices, Faculty of Physics and Electronic Science, Hubei University, 430062, Wuhan, P. R. China.

*To whom correspondence should be addressed.

E-mail: caofeifei@mail.hzau.edu.cn (Fei-Fei Cao)

Captions for Supporting Information

Theoretical calculation details; Table S1-S4; Figure S1-S25. (PDF)

Video S1: $Fe_{17.5\%}$-Ni_3S_2/NF||$Fe_{17.5\%}$-Ni_3S_2/NF water electrolyzer at high current density. (AVI)

Video S2: $Fe_{17.5\%}$-Ni_3S_2/NF||$Fe_{17.5\%}$-Ni_3S_2/NF water electrolyzer powered by a commercial D-type battery. (AVI)

Theoretical calculations

The surface of N_3S_2 has been cut along the (-2 1 0) direction, and the vacuum space along the z direction is set to be 15 Å, which is enough to avoid interaction between the two neighboring images. One Fe atom has replaced one Ni atom at sites 1, 2 or 3, respectively (Figure S14), and only the most stable replaced site has been considered. One H atom has been absorbed on the surface of substrates. The first principles calculations in the framework of density functional theory, including structural, electronic performances, were carried out based on the Cambridge Sequential Total Energy Package known as CASTEP.[1] The exchange–correlation functional under the generalized gradient approximation (GGA)[2] with norm-conserving pseudopotentials and Perdew–Burke–Ernzerhof functional was adopted to describe the electron–electron interaction.[3] An energy cutoff of 750 eV was used and a k-point sampling set of 5 × 4 × 1 were tested to be converged. A force tolerance of 0.01 eV $Å^{-1}$, energy tolerance of 5.0×10^{-7} eV per atom and maximum displacement of 5.0×10^{-4} Å were considered. Each atom in the storage models is allowed to relax to the minimum in the enthalpy without any constraints.

The substituted energy E_{sub} of systems was defined as:

$$E_{sub} = E_{Ni3S2} - E_{Ni3S2/Fe} \quad (1)$$

where E_{Ni3S2} and $E_{Ni3S2/Fe}$ denote the energy of undoped and doped surface or bulk.

Adsorption energy ΔE of H atom on the surface of substrates was defined as:

$$\Delta E = E_{*H} - (E_{*} + E_{H}) \quad (2)$$

where *H and * denote the adsorption of H atom on substrates and the bare substrates, E_H denotes the half of energy of H_2.

Free energy change ΔG of the reaction was calculated as the difference between the free energies of the initial and final states as shown below:

$$\Delta G = \Delta E + \Delta ZPE - T\Delta S \quad (3)$$

where E is the calculated energy by DFT, ZPE is the zero point energy, S denotes the entropy. The value of ($\Delta ZPE - T\Delta S$) is 0.28 eV,[4] so $\Delta G = \Delta E$ + 0.28eV.

Table S1 The comparison of catalytic performances for HER in 1 M KOH between $Fe_{17.5\%}$-Ni_3S_2/NF and other sulfide materials reported in the literature.

	η@10 mA cm-2 mV	η@20 mA cm-2 mV	η@100 mA cm-2 mV	Tafel slope mV dec^{-1}	Reference
$Fe_{17.5\%}$-Ni_3S_2/NF	47	142	232	95	This work
$Fe_{0.1}$-NiS_2 NA/Ti	~200	243	~310	108	5
Sn-Ni_3S_2/NF	137	~200	~320	148	6
MoO_x/ Ni_3S_2/NF	106		224	90	7
$CoMoS_3$ nanotubes	133	~170		105	8
$NiCo_2S_4$ NA/CC		~200	305	141	9
NiS/NF		158	~200	83	10
High-Index Faceted Ni_3S_2/NF	223	~300			11
$Ni_xCo_{3-x}S_4$/ Ni_3S_2/NF	136		258	107	12
V−Ni_3S_2−NW(V-doped Ni_3S_2)		203	~350	112	13
200-SMN/NF(Mo doped Ni_3S_2)			278	72.9	14
MoS_2/Ni_3S_2 heterostructures	110	~120		83.1	15
Ni_3S_2/NF covered with RGO	157	~200		92.8	16
Co_9S_8@NOSC-900	320			105	17
Ni–Co–MoS_2 nanoboxes	155	~170		51	18
CP/CTs/Co-S	190			131	19
$NiCo_2S_4$ NW/NF	210		~350	58.9	20
FNHNs/NF	140	~200		81.63	21
$Zn_{0.30}Co_{2.70}S_4$	85				22
Ni/NiS	230	~260		123.3	23
N-Ni_3S_2/NF	110	~160	~230		24
MoS_2−Ni_3S_2 HNRs/NF	98	~120	191	61	25
NL@NF-1	182			89	26
NiFeS-1/NF	180	~210		53	27
$Ni_{0.9}Fe_{0.1}PS_3$	72	~100		73	28
h-NiS_x/NF	60		175	99	29
Ni_3S_2/AT-Ni foam	200			107	30
NiS/NF	122		~200	69	31

Table S2 The comparison of exchange current density for HER in 1 M KOH between $Fe_{17.5\%}$-Ni_3S_2/NF and other materials reported in the literature.

	Exchange current density (j_0) mA cm^{-2}	Reference
$Fe_{17.5\%}$-Ni_3S_2/NF	0.77	This work
MoS_2/Ni_3S_2/NF	0.107	[32]
EG/Ni_3Se_2/Co_9S_8	0.27	[33]
CP/CTs/Co-S	0.39	[19]
a-Ni_3S_2@NPC	0.786	[34]
$MoNi_4$/NF	1.24	[35]
FeNi-N/CFC	1.21	[36]
EG/H-$Co_{0.85}$Se|P	0.17	[37]
np-$(Co_{0.52}Fe_{0.48})_2P$	0.12	[38]
EG/$Co_{0.85}$Se/NiFe-LDH	0.22	[39]
FeB_2	0.245	[40]
FeMnP/GNF	0.78	[41]

Table S3 Comparison of HER performance in 1.0 M PBS (pH=7) for $Fe_{17.5\%}$-Ni_3S_2/NF with other non-noble-metal HER catalysts.

	Current Density mA cm^{-2}	η / mV	Tafel slope mV dec^{-1}	Reference
$Fe_{17.5\%}$-Ni_3S_2/NF	10	145	114	This work
	100	337		
high-index-faceted Ni_3S_2/NF	10	170	n.a.	[11]
$FeMoS_4$ NRA/CC	10	204	128	[42]
a-Ni_3S_2@NPC	2	193	n.a.	[34]
$CoMoS_4$ NTA/CC	10	104	77	[43]
Co_9S_8/CC-2	10	175	n.a.	[44]
$Co_{0.6}Fe_{0.4}P$/CNT	10	105	78	[45]
CoP NW/Hb	100	~400	106	[46]
Co/CoP-5	50	~410	72.3	[47]
HF-MoSP-800	10	456	n.a.	[48]
CoB	10	251(0.5 M PBS)	75	[49]
Co-NRCNTs	10	540	n.a.	[50]

Table S4 The comparison of catalytic performances for OER in 1 M KOH between $Fe_{17.5\%}$-Ni_3S_2/NF and other sulfide materials reported in the literature.

	η@10 mA cm-2 mV	η@20 mA cm-2 mV	η@100 mA cm-2 mV	Tafel slope mV dec^{-1}	Reference
$Fe_{17.5\%}$-Ni_3S_2/NF	214	222	249	42	This work
Fe-Ni_3S_2/FeNi	282	~320		54	[51]
$Fe_{0.1}$-NiS_2 NA/Ti			231	43	[5]
$Fe_{11.8\%}$-Ni_3S_2/NF			253	65.5	[52]
MoO_x/Ni_3S_2/NF	136		310		[7]
200-SMN/NF(Mo doped Ni_3S_2)			~400	45.5	[14]
$Ni_xCo_{3-x}S_4$/Ni_3S_2/NF	160		320	95	[12]
MoS_2/Ni_3S_2 heterostructures	218		~290	88	[15]
High-Index Faceted Ni_3S_2/NF	260	~280			[11]
N-Ni_3S_2/NF			~340	70	[24]
MoS_2−Ni_3S_2 HNRs/NF	249		341	57	[25]
NiS/NF			~370	89	[10]
FNHNs/NF	290	320	445	62.38	[21]
Ni/NiS		~320	~390	109.8	[23]
$FeNiS_2$ NSs	310			46	[53]
NL@NF-1	340			150	[26]
NiFeS/NF	65		189	119.4	[54]
NiFeS-1/NF			230	55	[27]
Zn-Ni_3S_2/NF			300	87	[55]
$Ni_{0.9}Fe_{0.1}PS_3$		329		69	[28]
h-NiS_x/NF	180		220	96	[29]
NiS/NF		315		71	[31]
$CoMoS_3$ nanotubes	~320	~370			[8]
$NiCo_2S_4$ NA/CC		280	340	89	[9]
HF-MoSP-900	119				[48]
CP/CTs/Co-S	306			72	[19]
$NiCo_2S_4$ NW/NF	260			40	[20]
NiFeMo LDH/NF			~276		[56]
Ni_5Fe LDH@NF	210	~230	~270	59	[57]

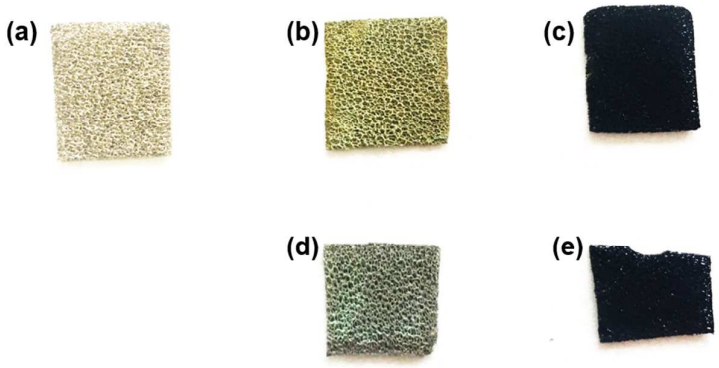

Figure S1 Photograph of (a) NF, (b) NiFe LDH/NF-3, (c) $Fe_{17.5\%}$-Ni_3S_2/NF, (d) $Ni(OH)_2 \cdot 0.75H_2O$/NF and (e) Ni_3S_2/NF.

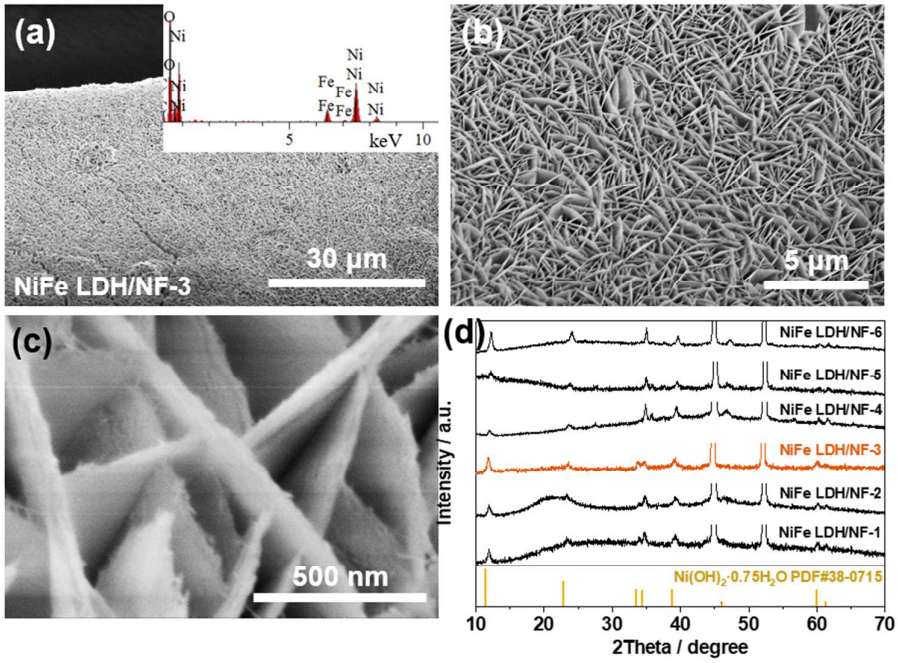

Figure S2 (a-c) SEM images of NiFe LDH/NF-3 and (d) XRD patterns of NiFe LDH/NF with different Fe content (see Table 1). Inset of (a) shows the EDS spectrum of NiFe LDH/NF-3.

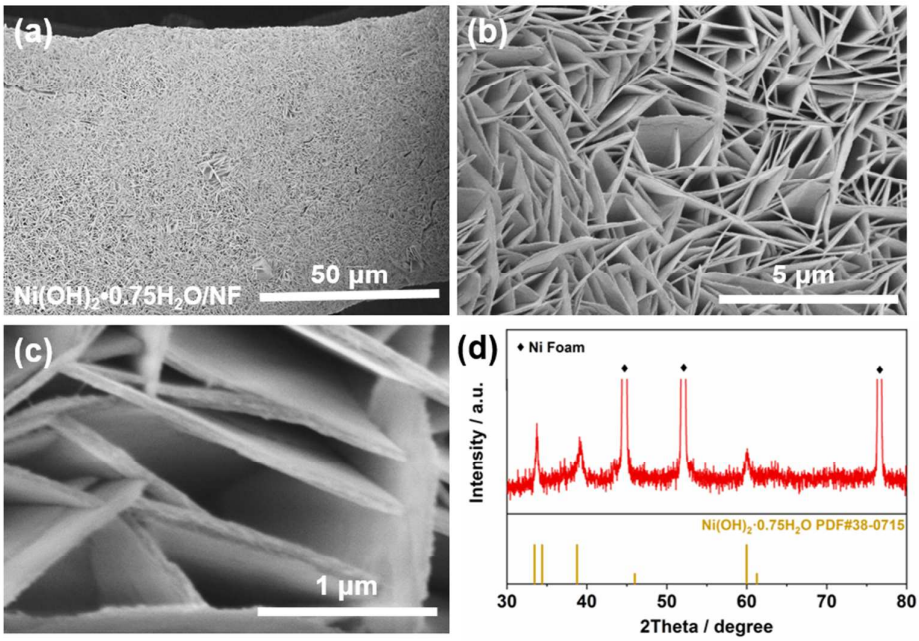

Figure S3 (a-c) SEM images and (d) XRD pattern of $Ni(OH)_2 \cdot 0.75H_2O$/NF.

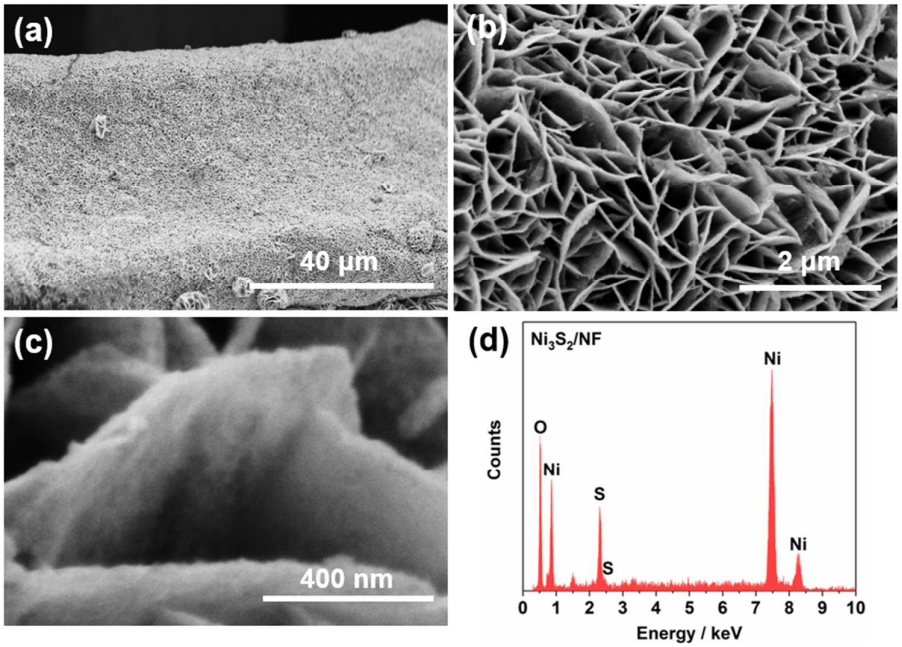

Figure S4 (a-c) SEM images and (d) EDS spectrum of Ni_3S_2/NF.

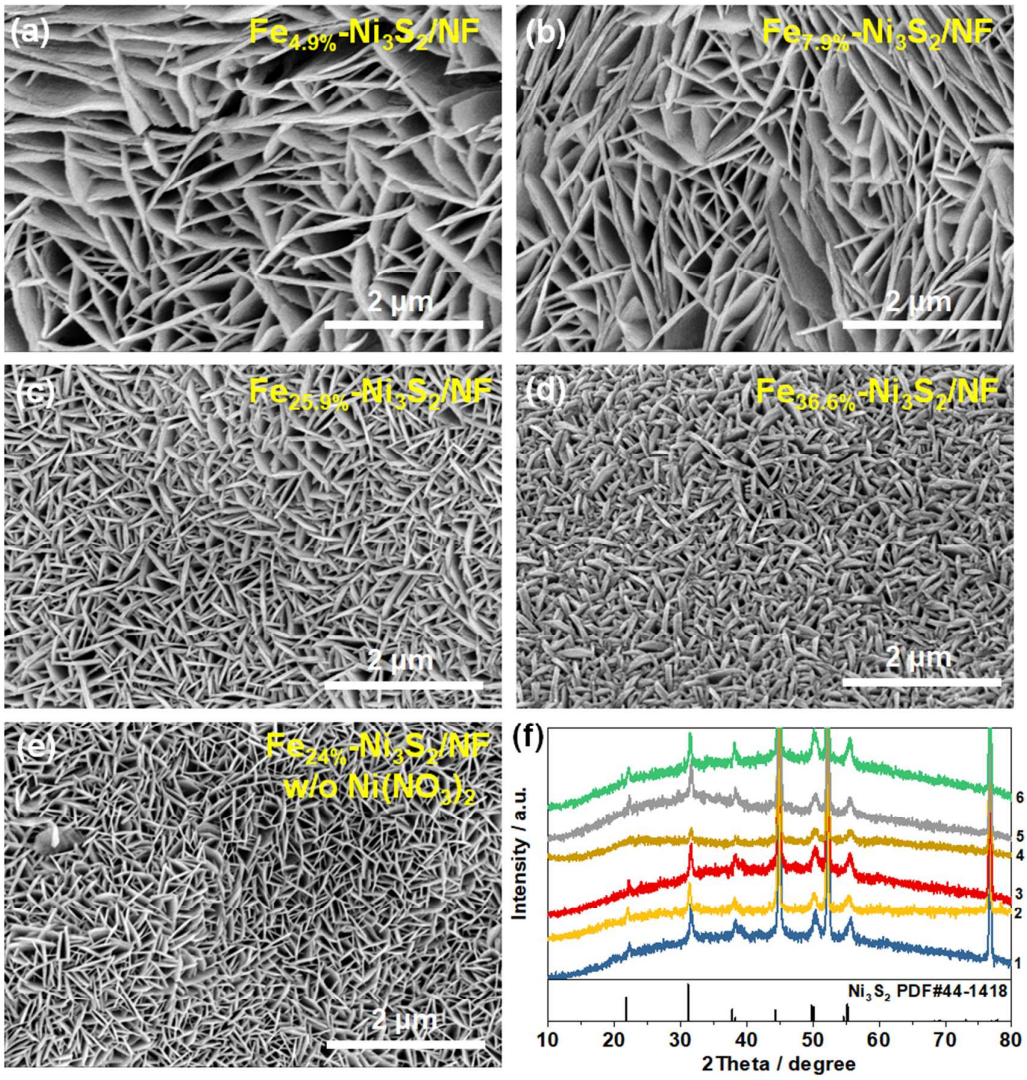

Figure S5 (a-e) SEM images of Fe- Ni_3S_2/NF with different Fe doping level. (f) XRD patterns for $Fe_{4.9\%}$- Ni_3S_2/NF (1), $Fe_{7.9\%}$- Ni_3S_2/NF (2), $Fe_{17.5\%}$- Ni_3S_2/NF (3), $Fe_{25.9\%}$- Ni_3S_2/NF (4), $Fe_{36.6\%}$- Ni_3S_2/NF (5) and $Fe_{24\%}$-Ni_3S_2/NF(w/o $Ni(NO_3)_2$) (6).

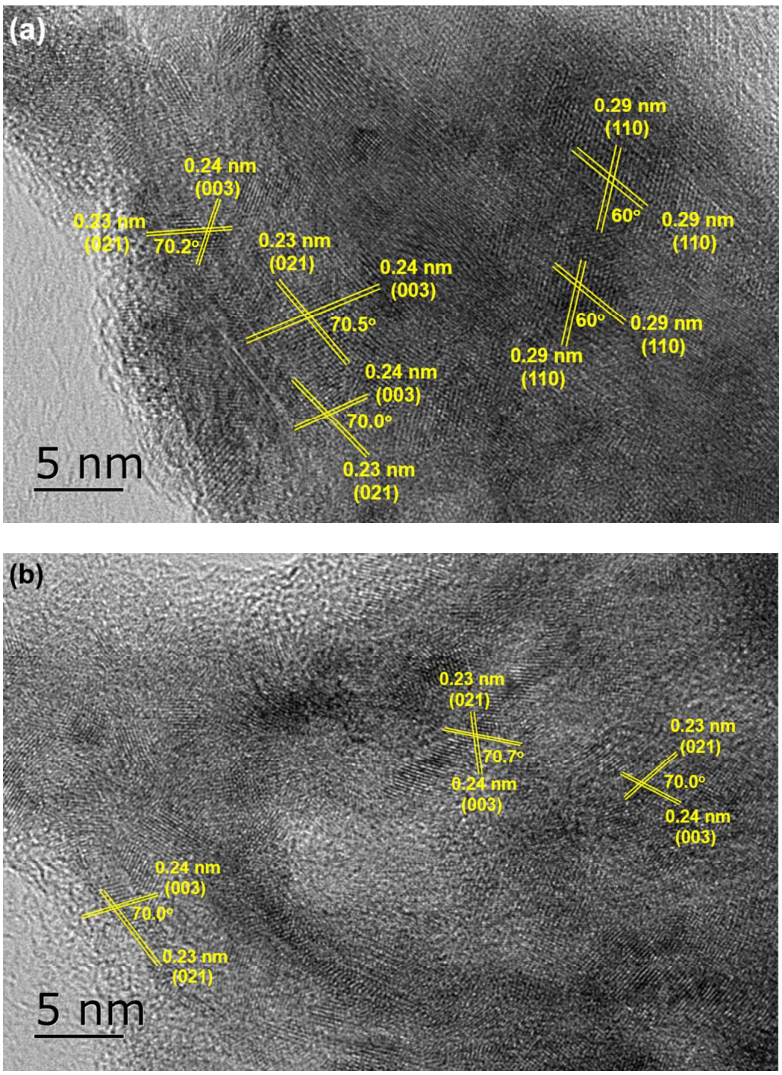

Figure S6 HRTEM images of $Fe_{17.5\%}$- Ni_3S_2 nanosheet.

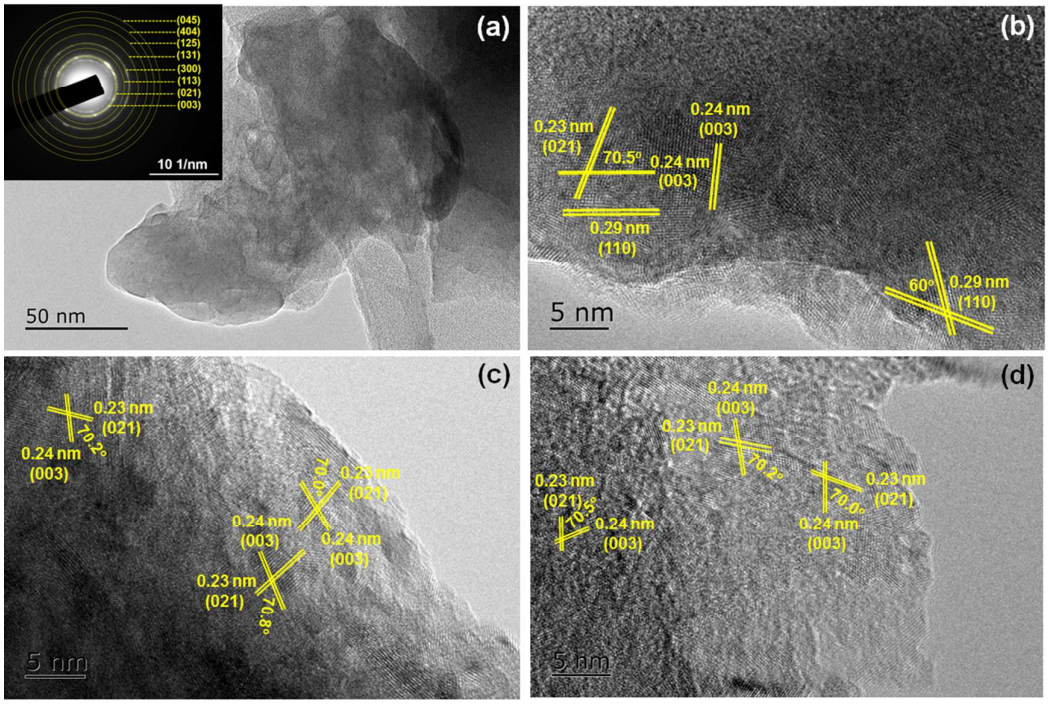

Figure S7 (a) TEM and (b) HRTEM images of Ni_3S_2 nanosheet.

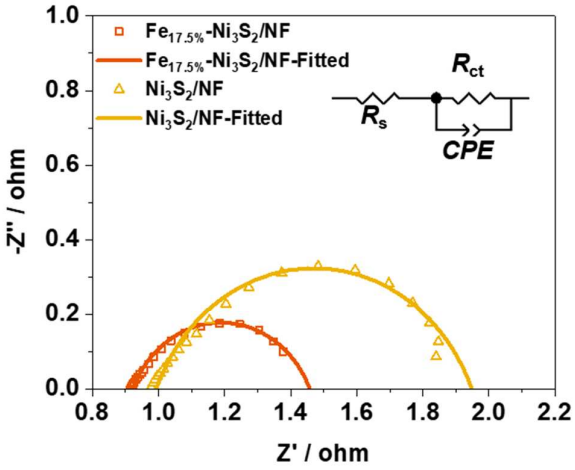

Figure S8 EIS curves of $Fe_{17.5\%}$-Ni_3S_2/NF and Ni_3S_2/NF recorded during hydrogen evolution at η = 333 mV (without *iR* correction). The inset shows the equivalent circuit.

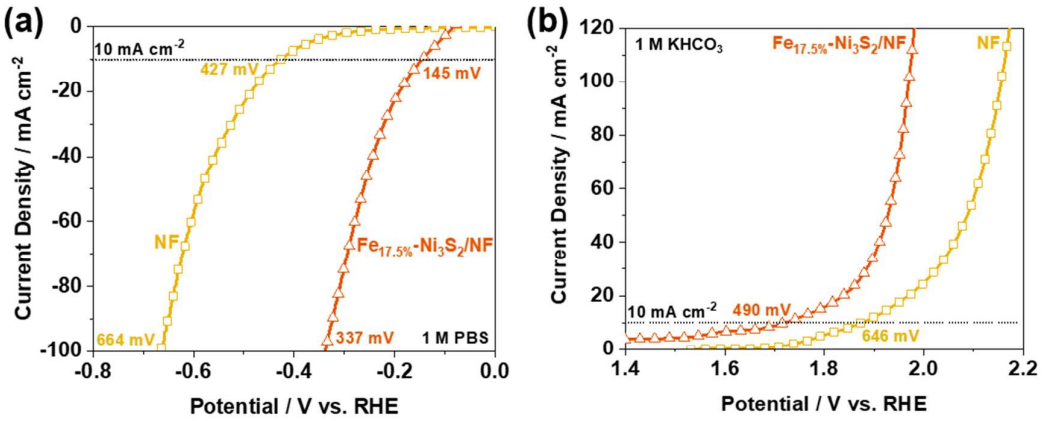

Figure S9 (a) HER polarization curves of $Fe_{17.5\%}$-Ni_3S_2/NF and NF in 1 M phosphate-bu□ered saline (PBS, pH=7). (b) OER polarization curves of $Fe_{17.5\%}$-Ni_3S_2/NF and NF in 1 M $KHCO_3$ (pH=8.3).

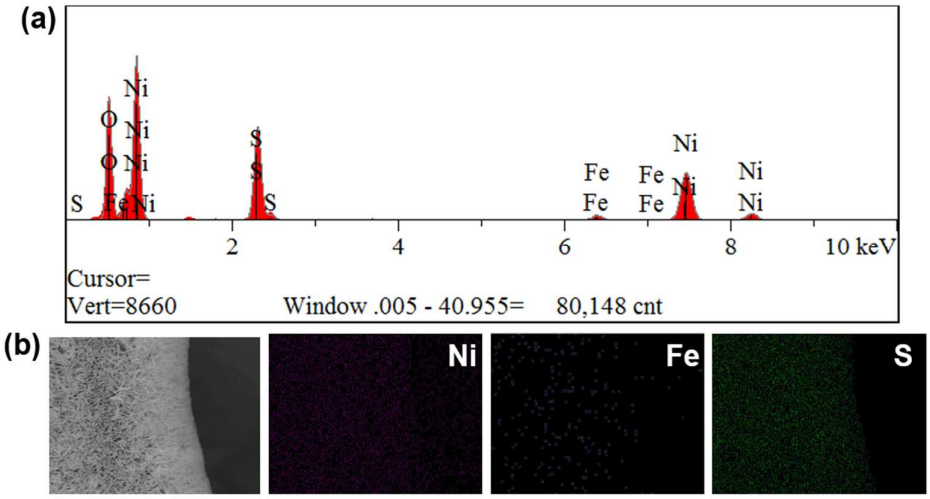

Figure S10 (a) EDS spectrum and (b) element mapping of $Fe_{17.5\%}$-Ni_3S_2/NF after HER catalysis for 20 h.

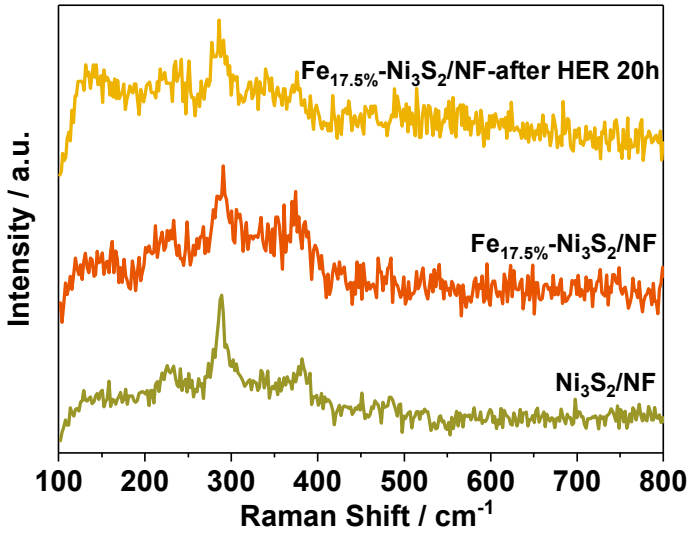

Figure S11 Raman spectra of Ni_3S_2/NF, $Fe_{17.5\%}$-Ni_3S_2/NF and $Fe_{17.5\%}$-Ni_3S_2/NF after durability testing for HER.

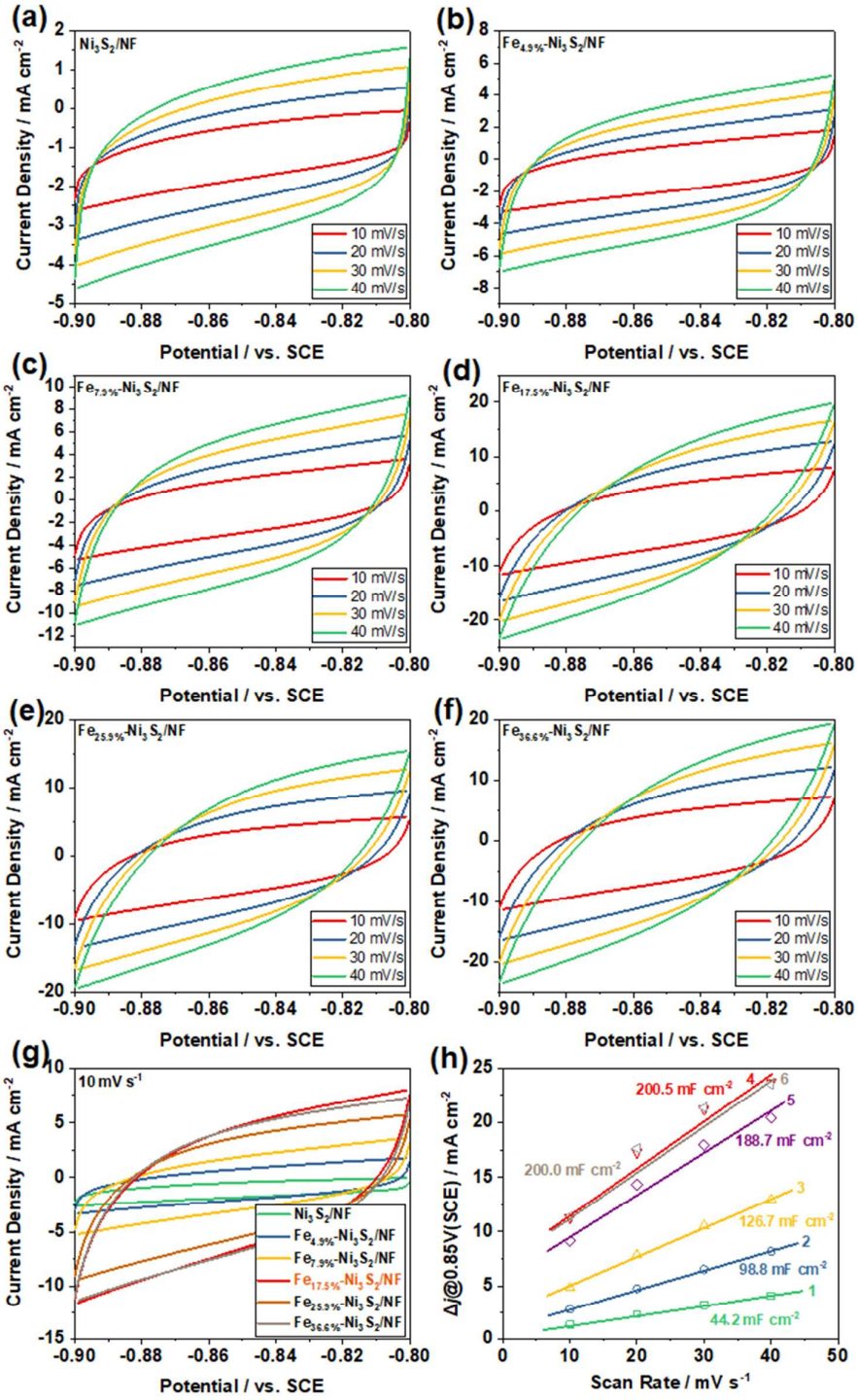

Figure S12 (a-g) CV curves of Ni_3S_2/NF and Fe-Ni_3S_2/NF with various Fe doping level. (h) Double layer capacitance (C_{dl}) for Ni_3S_2/NF (1), $Fe_{4.9\%}$- Ni_3S_2/NF (2), $Fe_{7.9\%}$- Ni_3S_2/NF (3), $Fe_{17.5\%}$- Ni_3S_2/NF (4), $Fe_{25.9\%}$- Ni_3S_2/NF (5) and $Fe_{36.6\%}$- Ni_3S_2/NF (6).

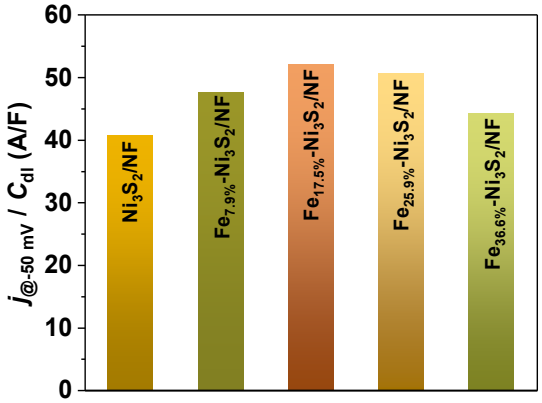

Figure S13 j/C_{dl} for various electrodes at η =50 mV during HER process.

(a)

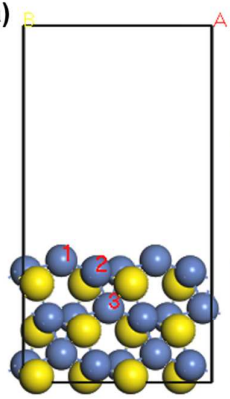

Doping site	Substituted energy / eV
1	0.74
2	-0.21
3	-0.02
Bulk	0.48

(b)

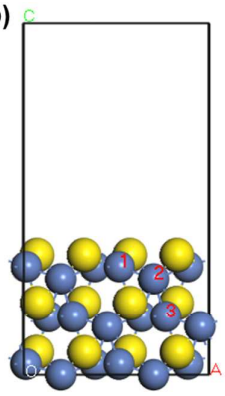

Doping site	Substituted energy / eV
1	0.28
2	0.18
3	0.32
Bulk	0.48

Figure S14 The side view of (a) Ni atom-terminated and (b) S atom-terminated Ni_3S_2 [58] plane with three possible doping sites of Fe atom and the corresponding substituted energy.

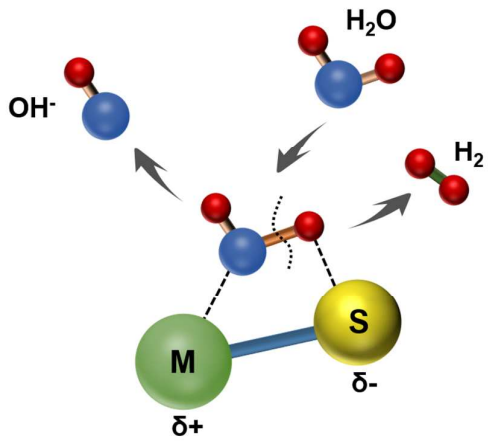

Figure S15 Schematic illustration of the speculated reaction mechanism for transition-metal sulfide during the HER process in alkaline media.

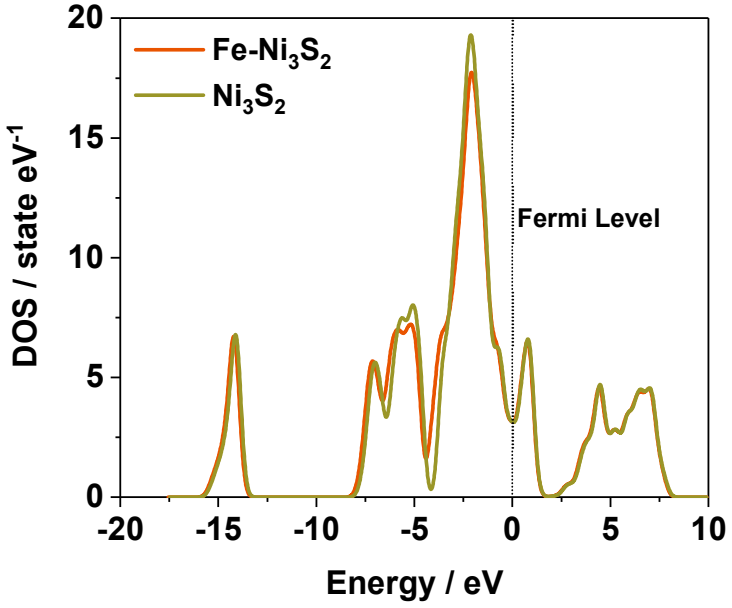

Figure S16 Calculated density of states of Fe-Ni_3S_2 and Ni_3S_2.

The continuous states crossing Fermi level suggests the metallic behavior of Ni_3S_2,[11, 51] which is maintained after Fe doping, indicating a high conductivity of materials, which is an important property for electrocatalyst.

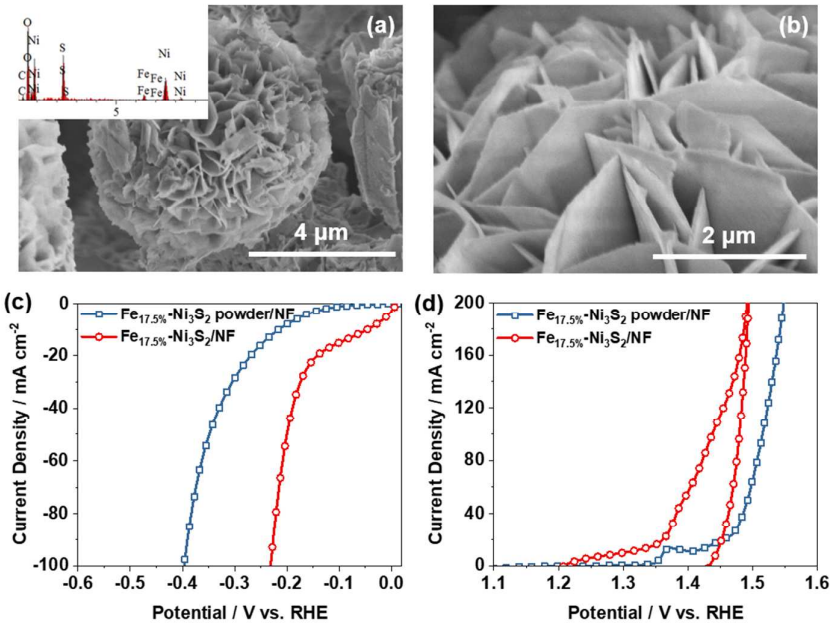

Figure S17 (a, b) SEM images of $Fe_{17.5\%}$-Ni_3S_2 powder. (c, d) Polarization curves for (c) HER and (d) OER of $Fe_{17.5\%}$-Ni_3S_2/NF and $Fe_{17.5\%}$-Ni_3S_2 powder/NF. $Fe_{17.5\%}$-Ni_3S_2 powder/NF was prepared by dipping slurry containing $Fe_{17.5\%}$-Ni_3S_2 powder, Nafion and ethanol on NF at the same catalyst loading with that of $Fe_{17.5\%}$-Ni_3S_2/NF.

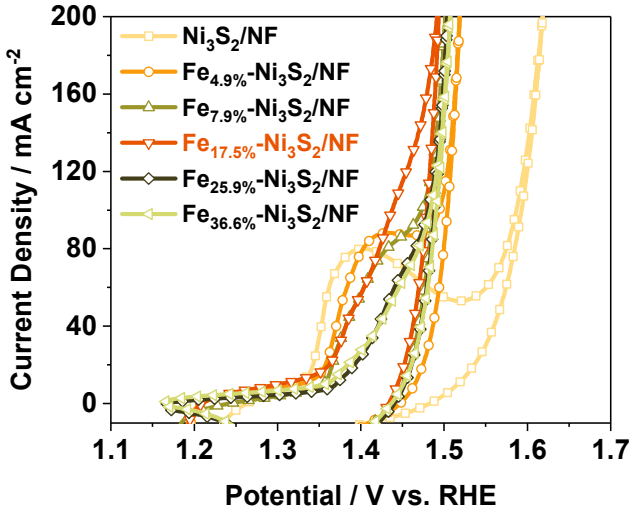

Figure S18 LSV curves of Fe-Ni_3S_2/NF with different Fe doping level for OER in 1 M KOH.

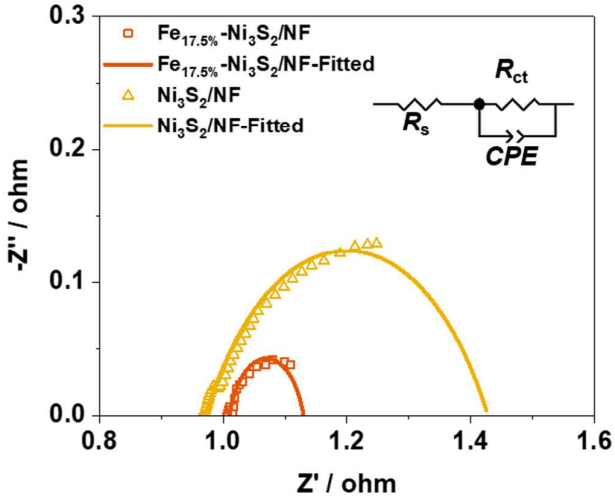

Figure S19 EIS curves of $Fe_{17.5\%}$-Ni_3S_2/NF and Ni_3S_2/NF recorded during oxygen evolution at η = 370 mV (without *iR* correction). The inset shows the equivalent circuit.

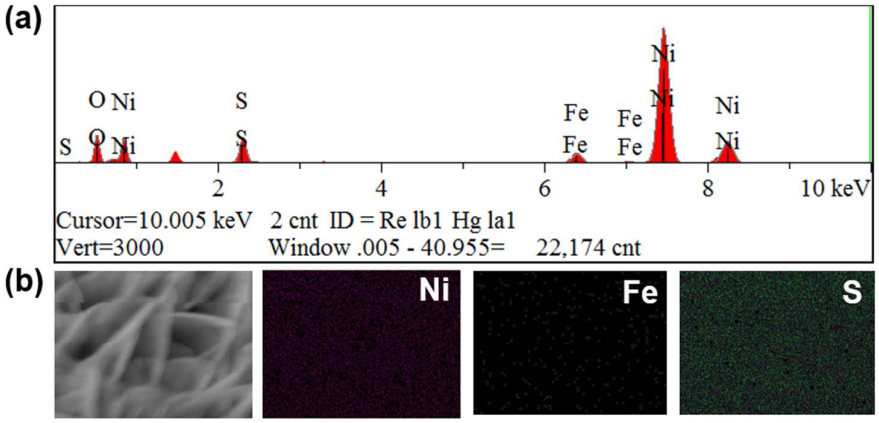

Figure S20 (a) EDS spectrum and (b) element mapping of $Fe_{17.5\%}$-Ni_3S_2/NF after OER catalysis for 20 h.

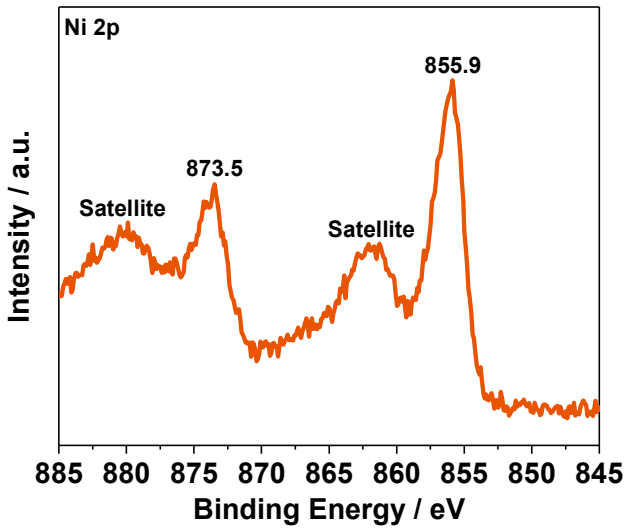

Figure S21 High-resolution Ni 2p XPS spectrum for $Fe_{17.5\%}$-Ni_3S_2/NF after OER catalysis for 20 h.

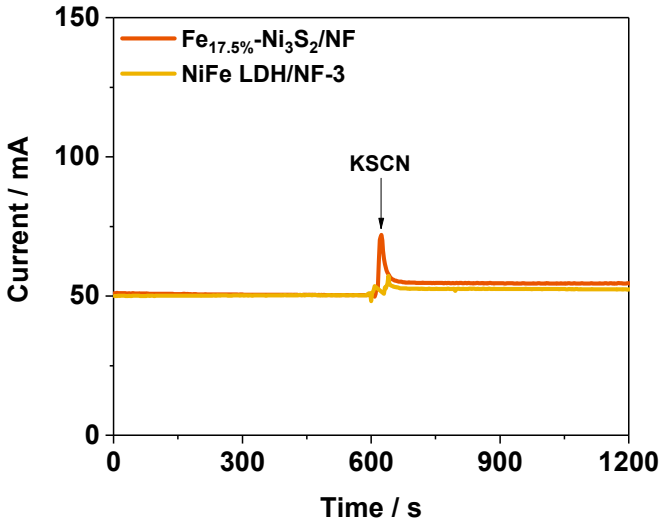

Figure S22 The effect of KSCN on the OER current of $Fe_{17.5\%}$-Ni_3S_2/NF and Ni_3S_2/NF under potentiostatic conditions.

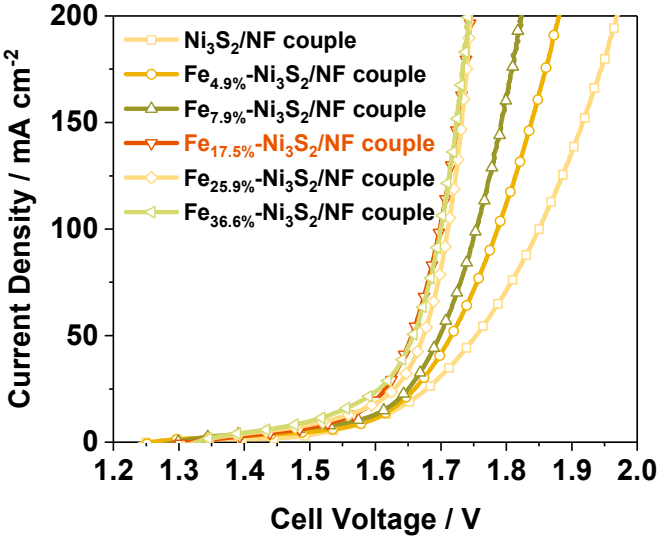

Figure 23 Polarization curves of Ni_3S_2/NF and Fe-Ni_3S_2/NF water electrolyzers in 1 M KOH at a scan rate of 5 mV s^{-1}; the curves are shown after *iR* correction.

Figure S24 Photograph of electrolytic cell after durability testing for Pt/C||IrO_x couple. The black powder at the bottom may be the catalyst peeled off from the NF substrate caused by the impact of generated gas bubbles.

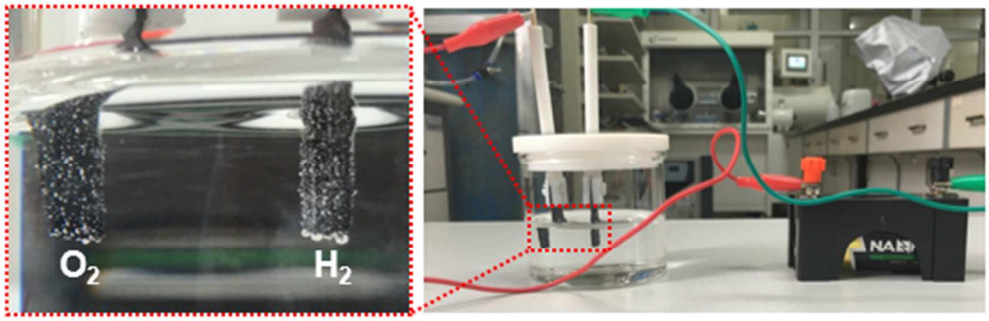

Figure S25 $Fe_{17.5\%}$-Ni_3S_2/NF||$Fe_{17.5\%}$-Ni_3S_2/NF electrolyzer powered by a commercial D-size battery (~1.5 V) in 1 M KOH.

References of Supporting Information

(1) Segall, M. D.; Lindan, P. J. D.; Probert, M. J.; Pickard, C. J.; Hasnip, P. J.; Clark, S. J.; Payne, M. C. First-principles simulation: ideas, illustrations and the CASTEP code. *J. Phys. Condes. Matter* **2002**, *14*, 2717-2744.

(2) Perdew, J. P.; Burke, K.; Ernzerhof, M. Generalized Gradient Approximation Made Simple. *Phys. Rev. Lett.* **1996**, *77*, 3865-3868.

(3) Hamann, D. R.; Schlüter, M.; Chiang, C. Norm-Conserving Pseudopotentials. *Phys. Rev. Lett.* **1979**, *43*, 1494-1497.

(4) Voiry, D.; Yamaguchi, H.; Li, J.; Silva, R.; Alves, D. C. B.; Fujita, T.; Chen, M.; Asefa, T.; Shenoy, V. B.; Eda, G.; Chhowalla, M. Enhanced catalytic activity in strained chemically exfoliated WS_2 nanosheets for hydrogen evolution. *Nat. Mater.* **2013**, *12*, 850-855.

(5) Yang, N.; Tang, C.; Wang, K. Y.; Du, G.; Asiri, A. M.; Sun, X. P. Iron-doped nickel disulfide nanoarray: A highly efficient and stable electrocatalyst for water splitting. *Nano Res.* **2016**, *9*, 3346-3354.

(6) Yu, J.; Ma, F.-X.; Du, Y.; Wang, P.-P.; Xu, C.-Y.; Zhen, L. In Situ Growth of Sn-Doped Ni_3S_2 Nanosheets on Ni Foam as High-Performance Electrocatalyst for Hydrogen Evolution Reaction. *ChemElectroChem* **2017**, *4*, 594-600.

(7) Wu, Y.; Li, G. D.; Liu, Y.; Yang, L.; Lian, X.; Asefa, T.; Zou, X. Overall Water Splitting Catalyzed Efficiently by an Ultrathin Nanosheet-Built, Hollow Ni_3S_2-Based Electrocatalyst. *Adv. Funct. Mater.* **2016**, *26*, 4839-4847.

(8) Guo, J.; Zhang, X.; Sun, Y.; Tang, L.; Zhang, X. Self-template synthesis of hierarchical $CoMoS_3$ nanotubes constructed of ultrathin nanosheets for robust water electrolysis. *J. Mater. Chem. A* **2017**, *5*, 11309-11315.

(9) Liu, D.; Lu, Q.; Luo, Y.; Sun, X.; Asiri, A. M. $NiCo_2S_4$ nanowires array as an efficient bifunctional electrocatalyst for full water splitting with superior activity. *Nanoscale* **2015**, *7*, 15122-15126.

(10) Zhu, W.; Yue, X.; Zhang, W.; Yu, S.; Zhang, Y.; Wang, J.; Wang, J. Nickel sulfide microsphere film on Ni foam as an efficient bifunctional electrocatalyst for overall water splitting. *Chem. Commun.* **2016**, *52*, 1486-1489.

(11) Feng, L. L.; Yu, G.; Wu, Y.; Li, G. D.; Li, H.; Sun, Y.; Asefa, T.; Chen, W.; Zou, X. High-Index Faceted Ni3S2 Nanosheet Arrays as Highly Active and Ultrastable Electrocatalysts for Water Splitting. *J. Am. Chem. Soc.* **2015**, *137*, 14023-14026.

(12) Wu, Y.; Liu, Y.; Li, G. D.; Zou, X.; Lian, X.; Wang, D.; Sun, L.; Asefa, T.; Zou, X. Efficient electrocatalysis of overall water splitting by ultrasmall $NixCo_{3-x}S_4$ coupled Ni_3S_2 nanosheet arrays. *Nano Energy* **2017**, *35*, 161-170.

(13) Qu, Y.; Yang, M.; Chai, J.; Tang, Z.; Shao, M.; Kwok, C. T.; Yang, M.; Wang, Z.; Chua, D.; Wang, S.; Lu, Z.; Pan, H. Facile Synthesis of Vanadium-Doped Ni_3S_2 Nanowire Arrays as Active Electrocatalyst for Hydrogen Evolution Reaction. *ACS Appl. Mater. Interfaces* **2017**, *9*, 5959-5967.

(14) Cui, Z.; Ge, Y. C.; Chu, H.; Baines, R.; Dong, P.; Tang, J. H.; Yang, Y.; Ajayan, P. M.; Ye, M. X.; Shen, J. F. Controlled synthesis of Mo-doped Ni_3S_2 nano-rods: an efficient and stable electro-catalyst for water splitting. *J. Mater. Chem. A* **2017**, *5*, 1595-1602.

(15) Zhang, J.; Wang, T.; Pohl, D.; Rellinghaus, B.; Dong, R.; Liu, S.; Zhuang, X.; Feng, X. Interface Engineering of MoS_2/Ni_3S_2 Heterostructures for Highly Enhanced Electrochemical Overall-Water-Splitting Activity. *Angew. Chem. Int. Ed.* **2016**, *55*, 6702-6707.

(16) Lv, J. L.; Miura, H.; Yang, M.; Liang, T. X. Synthesis of Ni_3S_2 nanotube arrays on nickel foam by catalysis of thermal reduced graphene for hydrogen evolution reaction. *Appl. Surf. Sci.* **2017**, *399*, 769-774.

(17) Huang, S.; Meng, Y.; He, S.; Goswami, A.; Wu, Q.; Li, J.; Tong, S.; Asefa, T.; Wu, M. N-, O-, and S-Tridoped Carbon-Encapsulated Co_9S_8 Nanomaterials: Efficient Bifunctional Electrocatalysts for Overall Water Splitting. *Adv. Funct. Mater.* **2017**, *27*, 1606585.

(18) Yu, X.-Y.; Feng, Y.; Jeon, Y.; Guan, B.; Lou, X. W.; Paik, U. Formation of Ni–Co–MoS_2 Nanoboxes with Enhanced Electrocatalytic Activity for Hydrogen Evolution. *Adv. Mater.* **2016**, *28*, 9006-9011.

(19) Wang, J.; Zhong, H.-X.; Wang, Z.L.; Meng, F.L.; Zhang, X.B. Integrated Three-Dimensional Carbon Paper/Carbon Tubes/Cobalt-Sulfide Sheets as an Efficient Electrode for Overall Water Splitting. *ACS Nano* **2016**, *10*, 2342-2348.

(20) Sivanantham, A.; Ganesan, P.; Shanmugam, S. Hierarchical $NiCo_2S_4$ Nanowire Arrays Supported on Ni Foam: An Efficient and Durable Bifunctional Electrocatalyst for Oxygen and Hydrogen Evolution Reactions. *Adv. Funct. Mater.* **2016**, *26*, 4661-4672.

(21) Liu, J.; Yang, Y.; Ni, B.; Li, H.; Wang, X. Fullerene-Like Nickel Oxysulfide Hollow Nanospheres as Bifunctional Electrocatalysts for Water Splitting. *Small* **2017**, *13*, 1602637.

(22) Huang, Z. F.; Song, J.; Li, K.; Tahir, M.; Wang, Y. T.; Pan, L.; Wang, L.; Zhang, X.; Zou, J. J. Hollow Cobalt-Based Bimetallic Sulfide Polyhedra for Efficient All-pH-Value Electrochemical and Photocatalytic Hydrogen Evolution. *J. Am. Chem. Soc.* **2016**, *138*, 1359-1365.

(23) Chen, G. F.; Ma, T. Y.; Liu, Z. Q.; Li, N.; Su, Y. Z.; Davey, K.; Qiao, S. Z. Efficient and Stable Bifunctional Electrocatalysts Ni/Ni_xM_y (M = P, S) for Overall Water Splitting. *Adv. Funct. Mater.* **2016**, *26*, 3314-3323.

(24) Chen, P.; Zhou, T.; Zhang, M.; Tong, Y.; Zhong, C.; Zhang, N.; Zhang, L.; Wu, C.; Xie, Y. 3D Nitrogen-Anion-Decorated Nickel Sulfides for Highly Efficient Overall Water Splitting. *Adv. Mater.* **2017**, *29*, 1701584.

(25) Yang, Y.; Zhang, K.; Lin, H.; Li, X.; Chan, H. C.; Yang, L.; Gao, Q. MoS_2–Ni_3S_2 Heteronanorods as Efficient and Stable Bifunctional Electrocatalysts for Overall Water Splitting. *ACS Catal.* **2017**, *7*, 2357-2366.

(26) Zhu, T.; Zhu, L. L.; Wang, J.; Ho, G. W. In situ chemical etching of tunable 3D Ni_3S_2 superstructures for bifunctional electrocatalysts for overall water splitting. *J. Mater. Chem. A* **2016**, *4*, 13916-13922.

(27) Ganesan, P.; Sivanantham, A.; Shanmugam, S. Inexpensive electrochemical synthesis of nickel iron sulphides on nickel foam: super active and ultra-durable electrocatalysts for alkaline electrolyte membrane water electrolysis. *J. Mater. Chem. A* **2016**, *4*, 16394-16402.

(28) Song, B.; Li, K.; Yin, Y.; Wu, T.; Dang, L.; Cabán-Acevedo, M.; Han, J.; Gao, T.; Wang, X.; Zhang, Z.; Schmidt, J. R.; Xu, P.; Jin, S. Tuning Mixed Nickel Iron Phosphosulfide Nanosheet Electrocatalysts for Enhanced Hydrogen and Oxygen Evolution. *ACS Catal.* **2017**, *7*, 8549-8557.

(29) You, B.; Sun, Y. J. Hierarchically Porous Nickel Sulfide Multifunctional Superstructures. *Adv. Energy Mater.* **2016**, *6*, 1502333.

(30) Ouyang, C.; Wang, X.; Wang, C.; Zhang, X.; Wu, J.; Ma, Z.; Dou, S.; Wang, S. Hierarchically Porous Ni_3S_2 Nanorod Array Foam as Highly Efficient Electrocatalyst for Hydrogen Evolution Reaction and Oxygen Evolution Reaction. *Electrochim. Acta* **2015**, *174*, 297-301.

(31) Ren, J. T.; Yuan, Z. Y. Hierarchical Nickel Sulfide Nanosheets Directly Grown on Ni Foam: A

Stable and Efficient Electrocatalyst for Water Reduction and Oxidation in Alkaline Medium. *ACS Sustain. Chem. Eng.* **2017**, *5*, 7203-7210.
(32) Zhang, N.; Lei, J. Y.; Xie, J. P.; Huang, H. Y.; Yu, Y. MoS_2/Ni_3S_2 nanorod arrays well-aligned on Ni foam: a 3D hierarchical efficient bifunctional catalytic electrode for overall water splitting. *RSC Adv.* **2017**, *7*, 46286-46296.
(33) Hou, Y.; Qiu, M.; Nam, G.; Kim, M. G.; Zhang, T.; Liu, K.; Zhuang, X.; Cho, J.; Yuan, C.; Feng, X. Integrated Hierarchical Cobalt Sulfide/Nickel Selenide Hybrid Nanosheets as an Efficient Three-dimensional Electrode for Electrochemical and Photoelectrochemical Water Splitting. *Nano Lett* **2017**, *17*, 4202-4209.
(34) Yang, C.; Gao, M. Y.; Zhang, Q. B.; Zeng, J. R.; Li, X. T.; Abbott, A. P. In-situ activation of self-supported 3D hierarchically porous Ni_3S_2 films grown on nanoporous copper as excellent pH-universal electrocatalysts for hydrogen evolution reaction. *Nano Energy* **2017**, *36*, 85-94.
(35) Zhang, J.; Wang, T.; Liu, P.; Liao, Z.; Liu, S.; Zhuang, X.; Chen, M.; Zschech, E.; Feng, X. Efficient hydrogen production on $MoNi_4$ electrocatalysts with fast water dissociation kinetics. *Nat. Commun.* **2017**, *8*, 15437.
(36) Yan, F.; Wang, Y.; Li, K.; Zhu, C.; Gao, P.; Li, C.; Zhang, X.; Chen, Y. Highly Stable Three-Dimensional Porous Nickel-Iron Nitride Nanosheets for Full Water Splitting at High Current Densities. *Chem.-Eur. J.* **2017**, *23*, 10187-10194.
(37) Hou, Y.; Qiu, M.; Zhang, T.; Zhuang, X.; Kim, C. S.; Yuan, C.; Feng, X. Ternary Porous Cobalt Phosphoselenide Nanosheets: An Efficient Electrocatalyst for Electrocatalytic and Photoelectrochemical Water Splitting. *Adv. Mater.* **2017**, *29*, 1701589.
(38) Tan, Y.; Wang, H.; Liu, P.; Shen, Y.; Cheng, C.; Hirata, A.; Fujita, T.; Tang, Z.; Chen, M. Versatile nanoporous bimetallic phosphides towards electrochemical water splitting. *Energy Environ. Sci.* **2016**, *9*, 2257-2261.
(39) Hou, Y.; Lohe, M. R.; Zhang, J.; Liu, S.; Zhuang, X.; Feng, X. Vertically oriented cobalt selenide/NiFe layered-double-hydroxide nanosheets supported on exfoliated graphene foil: an efficient 3D electrode for overall water splitting. *Energy Environ. Sci.* **2016**, *9*, 478-483.
(40) Li, H.; Wen, P.; Li, Q.; Dun, C.; Xing, J.; Lu, C.; Adhikari, S.; Jiang, L.; Carroll, D. L.; Geyer, S. M. Earth-Abundant Iron Diboride (FeB_2) Nanoparticles as Highly Active Bifunctional Electrocatalysts for Overall Water Splitting. *Adv. Energy Mater.* **2017**, *7*, 1700513.
(41) Zhao, Z.; Schipper, D. E.; Leitner, A. P.; Thirumalai, H.; Chen, J. H.; Xie, L.; Qin, F.; Alam, M. K.; Grabow, L. C.; Chen, S.; Wang, D.; Ren, Z.; Wang, Z.; Whitmire, K. H.; Bao, J. Bifunctional metal phosphide FeMnP films from single source metal organic chemical vapor deposition for efficient overall water splitting. *Nano Energy* **2017**, *39*, 444-453.
(42) Ren, X.; Wang, W.; Ge, R.; Hao, S.; Qu, F.; Du, G.; Asiri, A. M.; Wei, Q.; Chen, L.; Sun, X. An amorphous $FeMoS_4$ nanorod array toward efficient hydrogen evolution electrocatalysis under neutral conditions. *Chem. Commun.* **2017**, *53*, 9000-9003.
(43) Wang, W. Y.; Ren, X.; Hao, S.; Liu, Z. A.; Xie, F. Y.; Yao, Y. D.; Asiri, A. M.; Chen, L.; Sun, X. P. Self-Templating Construction of Hollow Amorphous $CoMoS_4$ Nanotube Array towards Efficient Hydrogen Evolution Electrocatalysis at Neutral pH. *Chem. Eur. J.* **2017**, *23*, 12718-12723.
(44) Feng, L. L.; Fan, M.; Wu, Y.; Liu, Y.; Li, G. D.; Chen, H.; Chen, W.; Wang, D.; Zou, X. Metallic Co_9S_8 nanosheets grown on carbon cloth as efficient binder-free electrocatalysts for the hydrogen evolution reaction in neutral media. *J. Mater. Chem. A* **2016**, *4*, 6860-6867.
(45) Zhang, X.; Zhang, X.; Xu, H.; Wu, Z.; Wang, H.; Liang, Y. Iron-Doped Cobalt Monophosphide

Nanosheet/Carbon Nanotube Hybrids as Active and Stable Electrocatalysts for Water Splitting. *Adv. Funct. Mater.* **2017**, *27*, 1606635.
(46) Huang, J.; Li, Y.; Xia, Y.; Zhu, J.; Yi, Q.; Wang, H.; Xiong, J.; Sun, Y.; Zou, G. Flexible cobalt phosphide network electrocatalyst for hydrogen evolution at all pH values. *Nano Res.* **2017**, *10*, 1010-1020.
(47) Xue, Z. H.; Su, H.; Yu, Q. Y.; Zhang, B.; Wang, H. H.; Li, X. H.; Chen, J. S. Janus Co/CoP Nanoparticles as Efficient Mott-Schottky Electrocatalysts for Overall Water Splitting in Wide pH Range. *Adv. Energy Mater.* **2017**, *7*, 1602355.
(48) Wu, A. P.; Tian, C. G.; Yan, H. J.; Jiao, Y. Q.; Yan, Q.; Yang, G. Y.; Fu, H. G. Hierarchical MoS_2@MoP core-shell heterojunction electrocatalysts for efficient hydrogen evolution reaction over a broad pH range. *Nanoscale* **2016**, *8*, 11052-11059.
(49) Gupta, S.; Patel, N.; Miotello, A.; Kothari, D. C. Cobalt-Boride: An efficient and robust electrocatalyst for Hydrogen Evolution Reaction. *J. Power Sources* **2015**, *279*, 620-625.
(50) Zou, X. X.; Huang, X. X.; Goswami, A.; Silva, R.; Sathe, B. R.; Mikmekova, E.; Asefa, T. Cobalt-Embedded Nitrogen-Rich Carbon Nanotubes Efficiently Catalyze Hydrogen Evolution Reaction at All pH Values. *Angew. Chem. Int. Ed.* **2014**, *53*, 4372-4376.
(51) Yuan, C. Z.; Sun, Z. T.; Jiang, Y. F.; Yang, Z. K.; Jiang, N.; Zhao, Z. W.; Qazi, U. Y.; Zhang, W. H.; Xu, A. W. One-Step In Situ Growth of Iron-Nickel Sulfide Nanosheets on FeNi Alloy Foils: High-Performance and Self-Supported Electrodes for Water Oxidation. *Small* **2017**, *13*, 1604161.
(52) Cheng, N. Y.; Liu, Q.; Asiri, A. M.; Xing, W.; Sun, X. P. A Fe-doped Ni_3S_2 particle film as a high-efficiency robust oxygen evolution electrode with very high current density. *J. Mater. Chem. A* **2015**, *3*, 23207-23212.
(53) Jiang, J.; Lu, S.; Gao, H.; Zhang, X.; Yu, H. Q. Ternary $FeNiS_2$ ultrathin nanosheets as an electrocatalyst for both oxygen evolution and reduction reactions. *Nano Energy* **2016**, *27*, 526-534.
(54) Dong, B.; Zhao, X.; Han, G. Q.; Li, X.; Shang, X.; Liu, Y. R.; Hu, W. H.; Chai, Y. M.; Zhao, H.; Liu, C. G. Two-step synthesis of binary Ni-Fe sulfides supported on nickel foam as highly efficient electrocatalysts for the oxygen evolution reaction. *J. Mater. Chem. A* **2016**, *4*, 13499-13508.
(55) Liu, Q.; Xie, L. S.; Liu, Z.; Du, G.; Asiri, A. M.; Sun, X. P. A Zn-doped Ni_3S_2 nanosheet array as a high-performance electrochemical water oxidation catalyst in alkaline solution. *Chem. Commun.* **2017**, *53*, 12446-12449.
(56) Han, N.; Zhao, F. P.; Li, Y. G. Ultrathin nickel-iron layered double hydroxide nanosheets intercalated with molybdate anions for electrocatalytic water oxidation. *J. Mater. Chem. A* **2015**, *3*, 16348-16353.
(57) Zhang, Y.; Shao, Q.; Pi, Y.; Guo, J.; Huang, X. A Cost-Efficient Bifunctional Ultrathin Nanosheets Array for Electrochemical Overall Water Splitting. *Small* **2017**, *13*, 1700355.
(58) Candelaria, S. L.; Shao, Y.; Zhou, W.; Li, X.; Xiao, J.; Zhang, J. G.; Wang, Y.; Liu, J.; Li, J.; Cao, G. Nanostructured carbon for energy storage and conversion. *Nano Energy* **2012**, *1*, 195-220.